Structural basis for Rab GTPase recognition and endosome tethering by the C_2H_2 zinc finger of Early Endosomal Autoantigen 1 (EEA1)

Ashwini Mishra, Sudharshan Eathiraj, Silvia Corvera, and David G. Lambright[1]

Program in Molecular Medicine and Department of Biochemistry and Molecular Pharmacology, University of Massachusetts Medical School, Worcester, MA 01605

Edited by Pietro De Camilli, Yale University and Howard Hughes Medical Institute (HHMI), New Haven, CT, and approved April 23, 2010 (received for review January 21, 2010)

Regulation of endosomal trafficking by Rab GTPases depends on selective interactions with multivalent effectors, including EEA1 and Rabenosyn-5, which facilitate endosome tethering, sorting, and fusion. Both EEA1 and Rabenosyn-5 contain a distinctive N-terminal C_2H_2 zinc finger that binds Rab5. How these C_2H_2 zinc fingers recognize Rab GTPases remains unknown. Here, we report the crystal structure of Rab5A in complex with the EEA1 C_2H_2 zinc finger. The binding interface involves all elements of the zinc finger as well as a short N-terminal extension but is restricted to the switch and interswitch regions of Rab5. High selectivity for Rab5 and, to a lesser extent Rab22, is observed in quantitative profiles of binding to Rab family GTPases. Although critical determinants are identified in both switch regions, Rab4-to-Rab5 conversion-of-specificity mutants reveal an essential requirement for additional substitutions in the proximal protein core that are predicted to indirectly influence recognition through affects on the structure and conformational stability of the switch regions.

Rab5 | effector | Rabenosyn-5 | endosome | structure

Rab GTPases regulate organelle biogenesis and vesicular transport by cycling between inactive (GDP-bound) and active (GTP-bound) states (1–4). After membrane targeting mediated by Rab GDI and conversion to the active form by GDP/GTP exchange factors (GEFs), Rab GTPases interact with effectors implicated in vesicular transport, tethering, and fusion (5–7). Rab5 controls endosome biogenesis, maturation, and fusion through multiple effectors (8–11). The Rab5 effector Early Endosomal Autoantigen 1 (EEA1) enhances endosome fusion and in combination with other soluble factors, including the Rab5 effector complex Rabenosyn-5·hVps45 and the Rab5 effector/GEF complex Rabaptin-5·Rabex-5, can substitute for cytosol in assays that reconstitute endosome fusion in vitro (12–15).

EEA1 is a long coiled coil homodimer with an N-terminal C_2H_2 zinc finger (ZF) and a C-terminal FYVE domain (16). The FYVE domain recognizes phosphatidyl inositol 3-phosphate (PI3P) and mediates PI3P-dependent recruitment to early endosomes (17–23). Low affinity Rab5 binding to the FYVE domain and proximal coiled coil is thought to enhance targeting to endosomes containing both Rab5 and PI3P (21). Higher affinity binding to the C_2H_2 ZF is proposed to facilitate long range tethering preceding formation of SNARE complexes required for membrane docking and fusion (1, 12, 24). Rabenosyn-5 also contains an N-terminal C_2H_2 ZF, which binds Rab5 with similar affinity, in addition to helical hairpin domains with distinct binding specificities for Rab4/Rab14 and Rab5/Rab22/Rab24 located within the central and C-terminal regions, respectively (24, 25).

Rab-effector recognition is considered a key factor with respect to the functional specificity of trafficking events and family-wide analyses indicate that the binding domains in effector proteins have evolved the capacity for highly selective recognition of small subsets of Rab GTPases (25, 26). Critical specificity determinants involving exposed/variable residues in the interaction epitopes of Rab GTPases have been identified and can be sufficient for effectors to distinguish Rab GTPases from the same phylogenetic group (25, 27–31). Whether these determinants are sufficient to account for effector recognition at the family level remains unclear.

Although well characterized as DNA-binding modules, little is known about the binding modalities and recognition properties of C_2H_2 ZFs that interact with proteins. To gain insight into Rab GTPase recognition by the EEA1 and Rabenosyn-5 C_2H_2 ZFs, we determined the crystal structure of the EEA1 C_2H_2 ZF, profiled the binding specificity for Rab GTPases, and used mutational analyses to characterize the underlying specificity determinants. Unexpectedly, we find that Rab-effector recognition depends not only on determinants in the switch/interswitch regions but also on nonconservative substitutions in the proximal protein core predicted to influence the active switch conformation.

Results

Structure of the C_2H_2 EEA1 Zinc Finger in Complex with Constitutively Active Rab5A. The Rab5 subfamily consists of three highly similar isoforms (Rab5A-C) with nearly indistinguishable properties in vitro. For simplicity, we refer specifically to individual isoforms only where necessary. Rab5 binding to the N terminus of EEA1 is mediated by the C_2H_2 ZF and does not require the hypervariable N- and C-terminal regions of Rab5 (24). Based on this, the constitutively active Q79L mutant of Rab5A (residues 15–184) was cocrystallized with the EEA1 C_2H_2 ZF (residues 36–69) and the structure solved by molecular replacement (Table S1). The asymmetric unit contains two independently refined Rab5:EEA1 complexes. Apart from small differences due to crystal packing, the mode of interaction as well as specific contacts are similar in both complexes (Fig. S1). The C_2H_2 ZF conforms to the "consensus" topology and adopts the expected ββα fold consisting of a β hairpin (β1–β2) and α helix (α1) cross-bridged by a Zn^{2+} ion. Unlike the archetypal DNA-binding module, the EEA1 C_2H_2 ZF has a negative electrostatic potential (pI ∼ 4.9) and a substantial nonpolar surface. Rab5 consists of a central beta sheet (β1–β6) surrounded by helices (α1–α5) as described in refs. 32–34.

As shown in Fig. 1*A*, a contiguous surface of the EEA1 C_2H_2 ZF formed by residues from the β1–β2 strands, α1 helix, and a short N-terminal extension, engages the switch and interswitch

Author contributions: A.M., S.E., S.C., and D.G.L. designed research; A.M. and S.E. performed research; S.C. contributed new reagents/analytic tools; A.M. and S.E. analyzed data; and A.M. and D.G.L. wrote the paper.

The authors declare no conflict of interest.

This article is a PNAS Direct Submission.

Data deposition: The atomic coordinates have been deposited in the Protein Data Bank (PDB ID code 3MJH and RCSB ID code rcsb058621).

[1]To whom correspondence should be addressed. E-mail: David.Lambright@umassmed.edu.

This article contains supporting information online at www.pnas.org/lookup/suppl/doi:10.1073/pnas.1000843107/-/DCSupplemental.

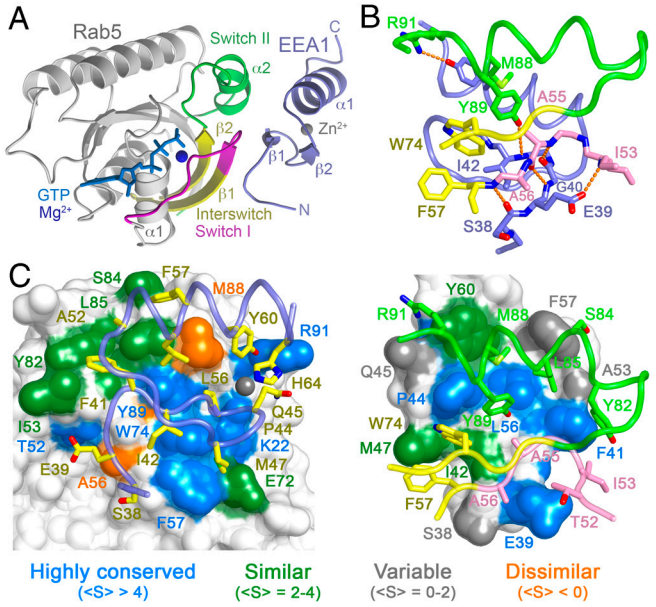

Fig. 1. Structural basis for Rab5 recognition by the EEA1 C_2H_2 ZF. (*A*) Ribbon rendering of the Rab5-C_2H_2 ZF complex. (*B*) Polar interactions in the Rab5-C_2H_2 ZF interface. Rendered *orange dashes* denote hydrogen bonds. (*C*) Nonpolar contacts in the Rab5-C_2H_2 ZF interface. Interfacial residues in Rab5A (*Left*) and EEA1 (*Right*) are shown as *spheres* covered by a semitransparent surface and colored according to conservation in paralogs (Rab5) or orthologs/paralogs (EEA1) as indicated. ⟨S⟩ refers to the mean substitution score calculated using a Blossum 62 substitution matrix.

regions of Rab5 through a predominantly nonpolar interface augmented by polar interactions (Fig. 1 *B* and *C*). The interaction epitope in Rab5 extends over invariant or highly similar nonpolar residues in switch I (Ile 53), interswitch (Phe 57 and Trp 74), and switch II (Tyr 82 and Arg 91) as well as residues in switch I (Ala 55 and Ala 56) and switch II (Leu 85 and Met 88) that are similar within the Rab5 group (Rab5, Rab21, and Rab22) defined by phylogenetic analyses (35) but dissimilar in other Rab GTPases. The corresponding epitope in the C_2H_2 ZF involves primarily residues that are invariant or similar in EEA1 and Rabenosyn-5 orthologs but not broadly conserved in C_2H_2 ZFs and is consistent with a mutational analysis in which the conserved residues were substituted with alanine (24). Notably, the two substitutions that showed no detectable binding involved Phe 41 and Ile 42 from the β1 strand. Phe 41 slots into a hydrophobic cleft bounded by Ile 53, Tyr 82, and Leu 85 from switch I/II while Ile 42 packs against Trp 74 in the interswitch region. Together, these interactions account for a substantial fraction of the nonpolar surface area buried on complex formation. Other alanine substitutions that showed substantial (14–42-fold) reduction in affinity involve Glu 39 from the N-terminal extension, Pro 44 from β1, Met 47 from β2, and Tyr 60 from α1. Glu 39 contacts Ala 56 in switch I as it extends to form a hydrogen bond with the backbone NH of Ile 53. Pro 44 wedges between Trp 74 in the interswitch region and Tyr 89 in switch II, Met 47 packs against Phe 57 in switch I, and Tyr 60 packs against Met 88 in switch II as its hydroxyl mediates a hydrogen bond with Arg 91. Conversely, the only conserved residue located outside the binding interface (Glu 61) exhibited a small (3-fold) decrease in affinity when mutated to alanine.

Modality of Rab GTPase Recognition by the EEA1 C_2H_2 Zinc Finger. In contrast to the mode of DNA recognition by C_2H_2 ZFs, in which the N terminus of the α1 helix inserts into the major groove, the EEA1 C_2H_2 ZF uses a distinct surface, involving residues supplied by the β1–β2 strands, α1 helix and N-terminal extension, to complement the convex surface presented by the switch-interswitch regions of Rab5. An analogous though less extensive surface comprised of residues from β1 and α1 interacts with a phage display-selected peptide extension in an engineered C_2H_2 ZF dimer (36) (see also Fig. S2*A*). Comparison with the Rabenosyn-5 helical hairpin-Rab22 complex reveals unexpected similarity in the respective binding interfaces (Fig. S2*B*, Fig. S3, Fig. S4). Despite unrelated folds, the C_2H_2 ZF and helical hairpin occupy nearly indistinguishable binding epitopes on Rab5 and exhibit high physiochemical similarity within the corresponding Rab-binding surfaces (Fig. S3, Fig. S4). Indeed, both modules provide: *i*) shape complementary nonpolar surfaces to engage the invariant aromatic residues in the switch/interswitch hydrophobic triad (Phe 57, Trp 74, and Tyr 89 in Rab5A); *ii*) a well defined nonpolar pocket for the switch II residues Leu 85 and Met 88 that are selectively conserved in the Rab5 phylogenetic group (PG5: Rab5, Rab21, and Rab22); *iii*) polar contacts for the backbone NH and side chain hydroxyl groups of the invariant switch I Phe 57 and switch II Tyr 89; and *iv*) residues that lie in van der Waals contact with the PG5-specific alanine or serine residue preceding the invariant switch I phenylalanine.

Specificity of the EEA1 and Rabenosyn-5 C_2H_2 Zinc Fingers for the Rab Family. The preceding observations indicate that Rab-binding domains (RBDs) with distinct folds can evolve similar Rab-interaction surfaces capable of recognizing a common epitope. However, small differences can give rise to distinct binding specificities, as observed for the central and C-terminal helical hairpins in Rabenonsyn-5 as well as the Rab-binding domains in Rab3 and Rab27 effectors (25, 37, 38). Therefore, a key question concerns the extent to which convergent structural similarity in the Rab-interaction surfaces confers the ability to recognize similar subsets of Rab GTPases. Likewise, whether the EEA1 and Rabenosyn-5 C_2H_2 ZFs have equivalent Rab specificity is not known. To address these questions, interactions with 31 purified Rab GTPases loaded with the nonhydrolyzeable GTP analog GppNHp were profiled using surface plasmon resonance (SPR). This collection includes most mammalian Rab proteins, except highly similar isoforms, and reflects the structural and functional diversity of the Rab family. As shown in Fig. 2 and Fig. S5, the EEA1 C_2H_2 ZF has the highest affinity for Rab5 ($K_d = 2.4$ μM) and 7-fold lower affinity for Rab22 ($K_d =$ 14 μM). For the remaining Rab GTPases, the SPR signal at the highest concentration (200 μM EEA1 C_2H_2 ZF) is <20% of that observed for Rab5. Similar results were obtained for the Rabenosyn-5 C_2H_2 ZF, which has highest affinity for Rab5 ($K_d = 4.8$ μM) and 12-fold lower affinity for Rab22 ($K_d =$ 63 μM). The absence of detectable binding for most Rab GTPases does not appear to be due to an inability to load GppNHp (Fig. S6). Thus, the EEA1 and Rabenosyn-5 C_2H_2 ZFs have a similar Rab specificity profile with a clear preference for Rab5 and substantially lower affinity for Rab22.

Structure-Based Mutational Analysis of Recognition Determinants. Given the physiochemical similarity of the Rab-interaction surfaces, the binding specificities of the C_2H_2 ZF and C-terminal helical hairpin modules likely reflect common determinants, including residues that are similar within interacting subsets but replaced by dissimilar residues in noninteracting Rab proteins. Although most residues in the binding epitope are broadly conserved, Ala 56 in switch I and Met 88 in switch II are conserved or similar in PG5 (Rab5, Rab21, and Rab22) but replaced by dissimilar residues in other Rab GTPases. Substitution of the equivalent Ala 57 in Rab5C with aspartic acid (the consensus residue) or glutamic acid (typical of the Rab4/Rab11 phylogenetic group; PG2) diminishes the affinity for the Rabenosyn-5 C-terminal helical hairpin by 10–50-fold (25). In the case of the EEA1 C_2H_2 ZF, the binding affinity is reduced by 36-fold for the aspartic acid substitution and is below the detection threshold ($K_d \gg 200$ μM) for the glutamic acid substitution (Fig. 3*B*). The side chain of Ala 56

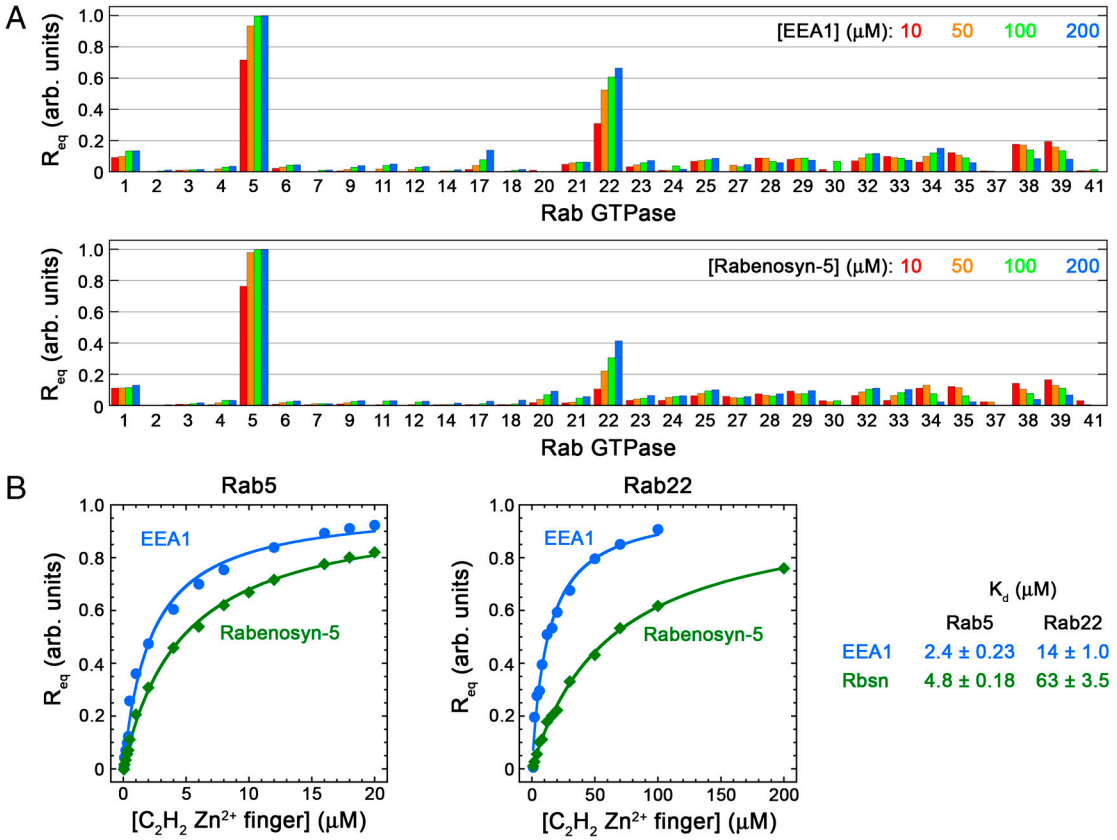

Fig. 2. The EEA1 and Rabenosyn-5 C_2H_2 ZFs bind selectively to Rab5 and Rab22. (*A*) Profile of C_2H_2 ZF binding to 31 Rab GTPases loaded with GppNHp. R_{eq} represents the equilibrium SPR response normalized to the maximum signal observed for binding to Rab5. (*B*) Quantitative analysis of 6xHis EEA1$_{36-91}$ and 6xHis Rbsn$_{1-70}$ binding to GST-Rab5A$_{18-185}$ (*Left*) and GST-Rab22A$_{2-169}$ (*Right*). *Solid lines* represent fitted model functions. R_{eq} represents the equilibrium SPR response normalized to the fitted maximum value for each dataset. Mean K_d values and standard deviations for 2–4 independent measurements are tabulated on the right.

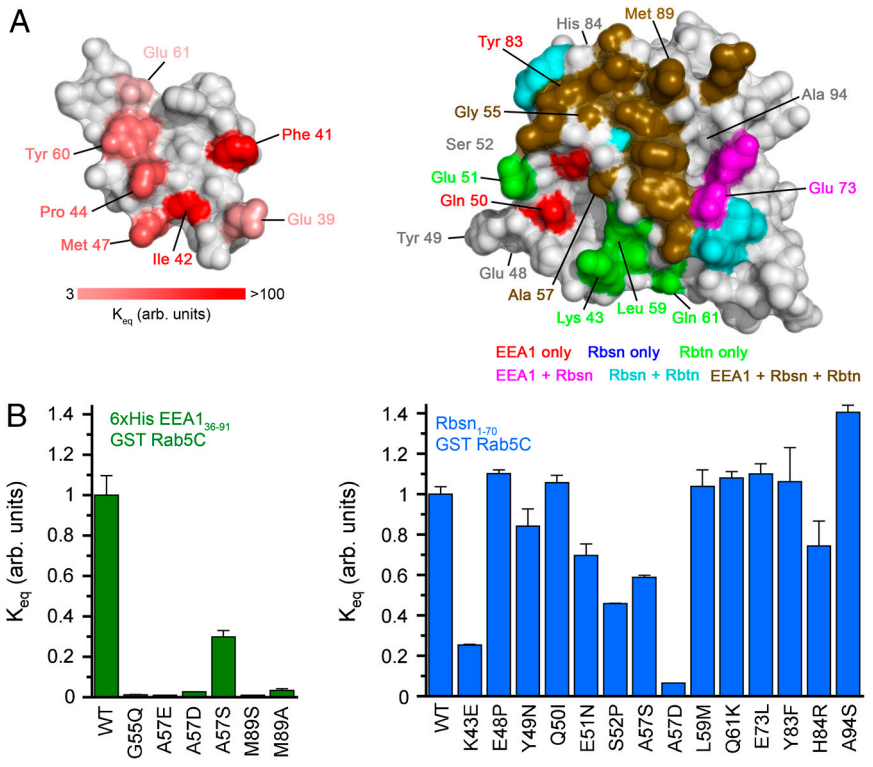

Fig. 3. Mutational analysis of interfacial recognition determinants. (*A*) Residues in the EEA1 C_2H_2 ZF (*Left*) colored as a gradient of equilibrium constants (K_{eq}) for binding of alanine mutants to Rab5C (24) and residues in Rab5A (*Right*) colored according to a comparison of interaction epitopes for the RBDs of EEA1, Rabenosyn-5, and Rabaptin-5. (*B*) Association constants (K_{eq}) for binding of: (*Left*) the EEA1 C_2H_2 ZF to Rab5C substituted with the consensus residue for the Rab family (A57D, M89A) or to the corresponding residue in Rab4 (A57E, M89S), Rab21 (G55Q), or Rab22 (A57S); and (*Right*) the Rbsn C_2H_2 ZF to Rab5C substituted with the consensus residue for the Rab family (A57D) or to the corresponding residue in Rab22A. Equilibrium constants were determined by SPR. Mean values and standard deviations for 2–4 measurements are plotted.

in Rab5A (note that Rab5A residue numbers are one less than in Rab5C) lies in van der Waals contact with the side chain of Glu 39 in the EEA1 C_2H_2 ZF such that substitution with larger acidic side chains would cause a steric clash expected to disrupt the polar interactions between the Glu 39 carboxylate group and the switch I backbone (Fig. 1 *B* and *C*). Met 89 in Rab5C is typically substituted by either alanine or serine/threonine in Rab GTPases that do not belong to PG5. Whereas alanine substitution has little effect on binding to the Rabenosyn-5 C-terminal helical hairpin, serine substitution reduces the affinity by 20-fold. Serine substitution eliminates binding to the EEA1 C_2H_2 ZF at concentrations up to 200 μM. Furthermore, the alanine substitution also results in a large decrease in binding affinity. The side chain of Met 88 in Rab5A is fully buried in a hydrophobic pocket in the C_2H_2 ZF (Fig. 1*C* and Fig. S4). The more severe affects on the affinity for the C_2H_2 ZF are consistent with partial solvent exposure of the corresponding nonpolar pocket in the Rab22 complex with the Rabenosyn-5 C-terminal helical hairpin (25).

Substitution of Gly 55 in Rab5C with glutamine as in Rab21 also greatly impairs binding to both the Rabenosyn-5 C-terminal helical hairpin and the EEA1 C_2H_2 ZF. In both cases, the affect can be attributed to van der Waals clashes resulting from introduction of a bulky residue within the binding interface (Fig. 1*C*). Finally, several Rab5C to Rab22A substitutions within or proximal to the binding interface reduce affinity for the Rabenosyn-5 C_2H_2 ZF by 2–4-fold (Fig. 3*B*). Evidently, no single substitution is sufficient to account for the 12-fold difference in affinity for Rab5 compared with Rab22.

Requirements for Conversion of Rab4 to Recognize Rab5 Effectors. Although the mutational analysis described above identified major recognition determinants in switch I and II, it is unclear whether they are sufficient or merely contribute to the observed specificity. To address this question, we generated a series of Rab4 variants with multiple substitutions to the corresponding residues in Rab5A (Fig. 4 *A* and *B*). Simultaneous substitution of the two critical determinants (hereafter Rab4to5+E44A +S76M) disrupts binding to the central helical hairpin of Rabenosyn-5 but is not sufficient to allow binding to Rab5 RBDs (Fig. 4*C*). Comparison of GTP-bound Rab4 and Rab5 structures suggests that the inability to bind Rab5 RBDs could be due to tertiary structural differences in the switch regions, which are most pronounced in switch II (Fig. 4*B*). These differences might in principle reflect substitutions within switch II; however, replacing the entire switch II region as well as switch I following the invariant threonine (hereafter Rab4to5+Sw) fails to confer binding to Rab5 RBDs (Fig. 4*C*). Analogous mutations in Rab21 also fail to confer binding to Rab5 RBDs (Fig. S7).

Further comparison of the Rab4 and Rab5 structures suggests that the active conformation of the switch regions could be influenced by structural differences in proximal elements. The largest differences occur in α3, which packs against switch II and is straight in Rab5 but kinked in Rab4 (Fig. 4*B*). It is likely that the structural differences in α3 reflect multiple substitutions in the protein core involving residues in α3 and potentially β4 and α4. Given that switch II also packs against β1, substitutions in β1 would be expected to influence the active structure and/or stability of switch II. Likewise, smaller differences in the active conformation of switch I appear to result from substitutions in α1 and β2. To test the hypothesis that effector specificity can be indirectly influenced by elements proximal to the switch regions, residues in α1, β1, β2, α3, and β4 of Rab4to5+Sw were collectively replaced by the corresponding residues of Rab5 (hereafter Rab4to5+Sw +core). These substitutions involve core residues that: *i*) directly contact the switch regions in the active state; and/or *ii*) are predicted to indirectly influence the active switch II conformation/stability through intramolecular interactions with α3. Rab4to5 +Sw+core loaded with GppNHp binds Rab5 RBDs with affinities comparable to Rab5 (Fig. 4*C*). Binding is not observed for the GDP-loaded form (Fig. 4*D*) or between GppNHp-loaded Rab4to5+Sw+core and the central helical hairpin of Rabenosyn-5 (Fig. S8). Finally, we note that Rab4to5+Sw+core has a high intrinsic exchange rate, which implies that additional substitutions would be required for complete functional conversion. Nevertheless, the exchange rate can be stimulated by the

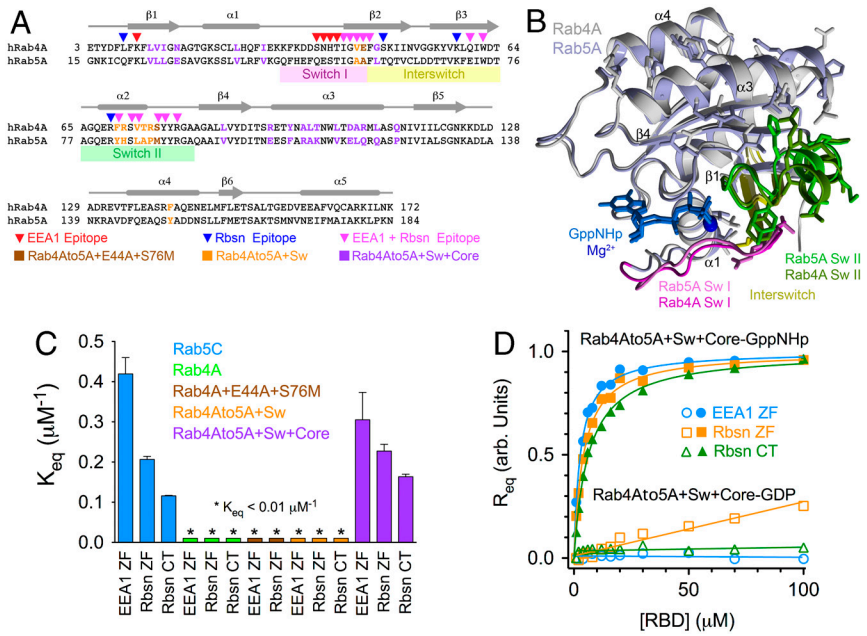

Fig. 4. Determinants for recognition of Rab5 vs. Rab4. (*A*) Sequence alignment of Rab4A and Rab5A indicating amino acid substitutions, secondary structural elements, functional regions and Rab5 effector binding epitoptes. (*B*) Comparison of Rab5A and Rab4A structures following superposition. Note tertiary structural differences in switch II and α3. (*C*) Binding affinity (K_{eq}) of Rab5 effector RBDs for Rab5C, Rab4A, and Rab4AtoRab5A chimeras determined by SPR. Mean values and standard deviations for 2–4 measurements are plotted. (*D*) Representative isotherms for equilibrium binding of Rab5 effector RBDs to the GDP- and GppNHp-bound forms of the Rab4to5+sw+core chimera. *Solid lines* represent fitted model functions.

Rab5/Rab21 GEF Rabex-5 with a catalytic efficiency similar to that for Rab5 (Fig. S9).

Discussion

We found that the EEA1 C_2H_2 ZF employs residues from β1–β2, α1, and a short N-terminal extension to recognize Rab5 and (to a lesser extent) Rab22 with high selectively. The interaction epitope on Rab5 is restricted to the switch/interswitch regions and overlaps extensively with the epitopes observed in Rab5 or Rab22 complexes with the structurally unrelated coiled or helical hairpin binding domains in Rabaptin-5 and Rabenosyn-5 (25, 39). Likewise, the interaction epitopes on the effector modules share high physiochemical similarity indicative of convergent evolution. Whereas C_2H_2 ZFs are widespread in prokaryotic and eukaryotic organisms, EEA1 and Rabenosyn-5 homologues are restricted to eukaryotes, with unambiguous orthologs in metazoans. Rabenosyn-5 orthologs can be identified in a broader range of metazoan genomes and potentially include the Vac1 protein in budding yeast (13). However, the C_2H_2 ZF in Vac1 contains a substitution predicted to disrupt Rab5 binding and does not bind to Rab5 (24). Thus, we suspect that Rab5-binding by a C_2H_2 ZF evolved first in an ancestral Rabenosyn-5 during elaboration of the endocytic system in multicellular organisms and was subsequently acquired by an ancestral EEA1 through gene duplication and fusion. Rab22 is the closest Rab5 paralog with respect to primary as well as tertiary structure (25, 35). Whereas Rab22 orthologs are restricted to metazoans, Rab5 orthologs are present in all eukaryotes, suggesting that Rab22 arose through duplication of an ancestral Rab5 gene. Apart from any potential functional role, the weaker interaction with Rab22 likely reflects incomplete divergence from Rab5.

How effectors recognize Rab GTPases represents an important but nontrivial problem. The nontrivial nature of effector recognition is due in part to the unpredictable contribution of variable elements and is further complicated by structural variability/plasticity in the active switch conformation (25, 27, 31, 33, 37, 38, 40, 41). Conversion of specificity through substitutions involving a limited set of surface residues within the interaction epitopes has been achieved in cases where the GTPases under consideration have similar tertiary structures (38, 42–44). In contrast, Rab4 differs substantially from Rab5 with respect to the tertiary structure of switch II and α3, which explains the additional requirement for substitutions in the protein core.

The observations reported here provide insight into the structural basis for endosome tethering, the modality/selectivity of protein recognition by C_2H_2 ZFs, and the multifactorial nature of Rab-effector recognition. In combination with the hypervariable regions, CDRs, and switch/interswitch determinants, substitutions in the protein core predicted to indirectly influence the structure/stability of the switch regions play a critical role in Rab-effector specificity. Additional studies are required to establish the extent to which the affects of the core substitutions are collective or attributable to determinants in specific structural elements.

Materials and Methods

Constructs. Constructs of human Rab5A (residues 15–184), the EEA1 C_2H_2 ZF (residues 36–69 and 36–91), and the Rabenosyn-5 C_2H_2 ZF (residues 1–70) were amplified and subcloned into modified pET28a or pET15b vectors for expression as 6xHis or 6xHis-SUMO fusions. Rab4A (residues 3–172) was cloned into a pGEX-6P-1 vector for expression as a GST fusion. Rab4A to Rab5A mutations in Rab4Ato5A+E44A+S76M and Rab4Ato5A+Sw were generated with the Quick Change Kit (Stratagene). Rab4Ato5A+Sw+Core mutations were generated by gene synthesis (Genescript) and subcloned into pGEX-6P-1.

Expression and Purification. BL21 (DE3) Codon plus RIL cells (Stratagene) transformed with expression plasmids were cultured in 2xYT media with either 100 mg/L ampicillin (modified pET15b and pGEX vectors) or 50 mg/L kanamycin (pET28a). Cells were grown at 22 °C to an OD_{600} of 0.4, induced with 0.05 mM IPTG for 16 h, and lysed in 50 mM Tris, pH 8.0, 100 mM NaCl, 5 mM $MgCl_2$, 0.1% 2-mercaptoethenol, 0.1 mM PMSF, 0.2 mg/mL lysozyme and 0.01 mg/mL DNAse I. After supplementing with 0.5% Triton X 100, lysates for GST fusions were clarified by centrifugation, incubated with glutathione sepharose beads, washed with 50 mM Tris, pH 8.0, 100 mM NaCl, 5 mM $MgCl_2$, 0.1% 2-mercaptoethenol, eluted with 10 mM reduced glutathione and further purified by gel filtration over Superdex 200. Lysates for 6xHis fusions were loaded onto Ni^{2+} sepharose columns (GE Healthcare), washed with 50 mM Tris, pH 8.0, 500 mM NaCl, 10 mM 2-mercaptoethenol, 15 mM imidazole and eluted with 300 mM imidazole in 50 mM Tris, pH 8.0, 100 mM NaCl, 10 mM 2-mercaptoethenol. 6xHis-SUMO fusions were digested with 6xHis-sumoase and further purified over Ni^{2+} sepharose, HiTrap Q HP ion exchange, and Superdex 200 (GE Healthcare). GST fusions of mouse $Rab5C_{18-185}$ and 6xHis Rabenosyn-$5_{728-784}$ were expressed and purified as described (25, 45).

Nucleotide Exchange. Rab GTPases (1–2 mg/mL) were incubated with a 25-fold excess of GppNHp or GDP in 20 mM Tris, pH 7.5, 150 mM NaCl, 5 mM EDTA for 12 h at 4 °C. After supplementing with 10 mM $MgCl_2$, excess nucleotide was removed by gel filtration over a 10 mL D-Salt column (Pierce).

Surface Plasmon Resonance. Surface plasmon resonance experiments were carried out on Biacore T100 and Biacore X instruments (GE Health Care). CM5 sensor chips were activated and coupled to anti-GST antibodies using the reagents and protocols provided by the manufacturer. For binding measurements all the proteins were exchanged into 20 mM Tris, pH 7.5, 150 mM NaCl, 2 mM $MgCl_2$ and 0.005% Surfactant P-20 and centrifuged at 1,500 rpm for 10 min. Reference and sample flow cells were loaded with equivalent amounts of GST or GST Rab fusion proteins, respectively. All subsequent injections were done at a flow rate of 0.02 mL/ min. Reference and sample sensograms were aligned, the reference signal subtracted, and the resulting equilibrium signal (R_{eq}) at each RBD concentration determined by averaging the data in the range from 20–40 s. The dissociation constant (K_d) was obtained by fitting with the Langmuir binding model $R_{eq} = R_{max}[RBD]/(K_d + [RBD])$.

Crystallization and Structure Determination. $Rab5A_{15-184}$ in complex with $EEA1_{36-69}$ was crystallized in hanging drops at 18 °C in 18% PEG 4000, 50 mM sodium acetate, pH 5.0, 0.2 M sodium-potassium phosphate, 10% glycerol. The crystals are in the primitive orthorhombic space group $P2_12_12_1$ with cell constants $a = 46.4$ Å, $b = 80.4$ Å, $c = 103.5$ Å, $\alpha = \beta = \gamma = 90°$. Crystals were harvested after 3 weeks, transferred to a cryostabilizer solution, flash frozen and maintained at 100 K in a nitrogen cryostream (Oxford Cryosystem). X-ray diffraction data were collected on a Rikagu RUH3R generator equipped with osmic mirrors and a MAR 345 detector. Data were processed with HKL 2000 and the structure solved by molecular replacement using AMoRe with Rab5C as a search model (46, 47). The initial crystallographic model was improved through iterative cycles of manual model building with Coot and refinement with ARP/wARP or Refmac5 (47). Structural figures were rendered with PyMOL (DeLano, W.L. The PyMOL Molecular Graphics System. (2008) DeLano Scientific LLC, Palo Alto, CA).

ACKNOWLEDGMENTS. We thank Marino Zerial for providing a full length Rabenosyn-5 clone, Maria Zapp for assistance with SPR experiments, and Anna Delprato for Rab5C mutants. SPR data were collected in the UMASS Center for AIDS Research Molecular Biology Core (UMASS CFAR 5P30 AI42845). This work was supported by an National Institutes of Health Grant (GM 056324).

1. Zerial M, McBride H (2001) Rab proteins as membrane organizers. *Nat Rev Mol Cell Biol* 2:107–117.
2. Pfeffer SR (2001) Rab GTPases: specifying and deciphering organelle identity and function. *Trends Cell Biol* 11:487–491.
3. Grosshans BL, Ortiz D, Novick P (2006) Rabs and their effectors: achieving specificity in membrane traffic. *Proc Natl Acad Sci USA* 103:11821–11827.
4. Stenmark H (2009) Rab GTPases as coordinators of vesicle traffic. *Nat Rev Mol Cell Biol* 10:513–525.
5. Goody RS, Rak A, Alexandrov K (2005) The structural and mechanistic basis for recycling of Rab proteins between membrane compartments. *Cell Mol Life Sci* 62:1657–1670.
6. Markgraf DF, Peplowska K, Ungermann C (2007) Rab cascades and tethering factors in the endomembrane system. *FEBS Lett* 581:2125–2130.

7. Cai H, Reinisch K, Ferro-Novick S (2007) Coats, tethers, Rabs, and SNAREs work together to mediate the intracellular destination of a transport vesicle. *Dev Cell* 12:671–682.
8. Gorvel JP, Chavrier P, Zerial M, Gruenberg J (1991) Rab5 controls early endosome fusion in vitro. *Cell* 64:915–925.
9. Bucci C, et al. (1992) The small GTPase Rab5 functions as a regulatory factor in the early endocytic pathway. *Cell* 70:715–728.
10. Stenmark H, Vitale G, Ullrich O, Zerial M (1995) Rabaptin-5 is a direct effector of the small GTPase Rab5 in endocytic membrane fusion. *Cell* 83:423–432.
11. Rink J, Ghigo E, Kalaidzidis Y, Zerial M (2005) Rab conversion as a mechanism of progression from early to late endosomes. *Cell* 122:735–749.
12. Simonsen A, et al. (1998) EEA1 links PI(3)K function to Rab5 regulation of endosome fusion. *Nature* 394:494–498.
13. Nielsen E, et al. (2000) Rabenosyn-5, a novel Rab5 effector, is complexed with hVPS45 and recruited to endosomes through a FYVE finger domain. *J Cell Biol* 151:601–612.
14. Christoforidis S, McBride HM, Burgoyne RD, Zerial M (1999) The Rab5 effector EEA1 is a core component of endosome docking. *Nature* 397:621–625.
15. Ohya T, et al. (2009) Reconstitution of Rab- and SNARE-dependent membrane fusion by synthetic endosomes. *Nature* 459:1091–1097.
16. Callaghan J, Simonsen A, Gaullier JM, Toh BH, Stenmark H (1999) The endosome fusion regulator early-endosomal autoantigen 1 (EEA1) is a dimer. *Biochem J* 338:539–543.
17. Stenmark H, Aasland R, Toh BH, D'Arrigo A (1996) Endosomal localization of the autoantigen EEA1 is mediated by a zinc-binding FYVE finger. *J Biol Chem* 271:24048–24054.
18. Patki V, Lawe DC, Corvera S, Virbasius JV, Chawla A (1998) A functional PtdIns(3) P-binding motif. *Nature* 394:433–434.
19. Gaullier JM, et al. (1998) FYVE fingers bind PtdIns(3)P. *Nature* 394:432–433.
20. Kutateladze TG, et al. (1999) Phosphatidylinositol 3-phosphate recognition by the FYVE domain. *Mol Cell* 3:805–811.
21. Lawe DC, Patki V, Heller-Harrison R, Lambright D, Corvera S (2000) The FYVE domain of early endosome antigen 1 is required for both phosphatidylinositol 3-phosphate and Rab5 binding. Critical role of this dual interaction for endosomal localization. *J Biol Chem* 275:3699–3705.
22. Dumas JJ, et al. (2001) Multivalent endosome targeting by homodimeric EEA1. *Mol Cell* 8:947–958.
23. Kutateladze T, Overduin M (2001) Structural mechanism of endosome docking by the FYVE domain. *Science* 291:1793–1796.
24. Merithew E, Stone C, Eathiraj S, Lambright DG (2003) Determinants of Rab5 interaction with the N terminus of early endosome antigen 1. *J Biol Chem* 278:8494–8500.
25. Eathiraj S, Pan X, Ritacco C, Lambright DG (2005) Structural basis of family-wide Rab GTPase recognition by rabenosyn-5. *Nature* 436:415–419.
26. Fukuda M, Kanno E, Ishibashi K, Itoh T (2008) Large scale screening for novel Rab effectors reveals unexpected broad Rab binding specificity. *Mol Cell Proteomics* 7:1031–1042.
27. Ostermeier C, Brunger AT (1999) Structural basis of Rab effector specificity: crystal structure of the small G protein Rab3A complexed with the effector domain of rabphilin-3A. *Cell* 96:363–374.
28. Eathiraj S, Mishra A, Prekeris R, Lambright DG (2006) Structural basis for Rab11-mediated recruitment of FIP3 to recycling endosomes. *J Mol Biol* 364:121–135.
29. Jagoe WN, et al. (2006) Crystal structure of Rab11 in complex with Rab11 family interacting protein 2. *Structure* 14:1273–1283.
30. Shiba T, et al. (2006) Structural basis for Rab11-dependent membrane recruitment of a family of Rab11-interacting protein 3 (FIP3)/Arfophilin-1. *Proc Natl Acad Sci USA* 103:15416–15421.
31. Burguete AS, Fenn TD, Brunger AT, Pfeffer SR (2008) Rab and Arl GTPase family members cooperate in the localization of the golgin GCC185. *Cell* 132:286–298.
32. Esters H, Alexandrov K, Constantinescu AT, Goody RS, Scheidig AJ (2000) High-resolution crystal structure of *S. cerevisiae* Ypt51(DeltaC15)-GppNHp, a small GTP-binding protein involved in regulation of endocytosis. *J Mol Biol* 298:111–121.
33. Merithew E, et al. (2001) Structural plasticity of an invariant hydrophobic triad in the switch regions of Rab GTPases is a determinant of effector recognition. *J Biol Chem* 276:13982–13988.
34. Zhu G, et al. (2003) High resolution crystal structures of human Rab5a and five mutants with substitutions in the catalytically important phosphate-binding loop. *J Biol Chem* 278:2452–2460.
35. Pereira-Leal JB, Seabra MC (2001) Evolution of the Rab family of small GTP-binding proteins. *J Mol Biol* 313:889–901.
36. Wang BS, Grant RA, Pabo CO (2001) Selected peptide extension contacts hydrophobic patch on neighboring zinc finger and mediates dimerization on DNA. *Nat Struct Biol* 8:589–593.
37. Chavas LM, et al. (2008) Elucidation of Rab27 recruitment by its effectors: structure of Rab27a bound to Exophilin4/Slp2-a. *Structure* 16:1468–1477.
38. Kukimoto-Niino M, et al. (2008) Structural basis for the exclusive specificity of Slac2-a/melanophilin for the Rab27 GTPases. *Structure* 16:1478–1490.
39. Zhu G, et al. (2004) Structural basis of Rab5-Rabaptin5 interaction in endocytosis. *Nat Struct Mol Biol* 11:975–983.
40. Constantinescu AT, et al. (2002) Rab-subfamily-specific regions of Ypt7p are structurally different from other RabGTPases. *Structure* 10:569–579.
41. Wu M, Wang T, Loh E, Hong W, Song H (2005) Structural basis for recruitment of RILP by small GTPase Rab7. *Embo J* 24:1491–1501.
42. Karnoub AE, Symons M, Campbell SL, Der CJ (2004) Molecular basis for Rho GTPase signaling specificity. *Breast Cancer Res Treat* 84:61–71.
43. Gao Y, Xing J, Streuli M, Leto TL, Zheng Y (2001) Trp(56) of rac1 specifies interaction with a subset of guanine nucleotide exchange factors. *J Biol Chem* 276:47530–47541.
44. Dong G, Medkova M, Novick P, Reinisch KM (2007) A catalytic coiled coil: structural insights into the activation of the Rab GTPase Sec4p by Sec2p. *Mol Cell* 25:455–462.
45. Delprato A, Merithew E, Lambright DG (2004) Structure, exchange determinants, and family-wide Rab specificity of the tandem helical bundle and Vps9 domains of Rabex-5. *Cell* 118:607–617.
46. Otwinowski Z, Minor W (1997) Processing of x-ray diffraction data collected in oscillation mode. *Methods Enzymol* 276:307–326.
47. CCP4 (1994) The CCP4 suite: programs for protein crystallography. *Acta Crystallogr D* 50:760–763.